ISSN 0023-1584, Kinetics and Catalysis, 2007, Vol. 48, No. 6, pp. 864–876. © MAIK "Nauka/Interperiodica" (Russia), 2007.
Published in Russian in Kinetika i Kataliz, 2007, Vol. 48, No. 6, pp. 924–938.

CARBON
IN CATALYSIS

Carbon Ceramic Composite Membranes for Catalytic Membrane Reactor Applications[1]

S. R. Tennison*[a], K. Arnott[a], and H. Richter[b]

[a] *MAST Carbon Technology Ltd, Henley Park, Surrey GU3 2AF*

[b] *Hermsdorfer Institut für Technische Keramik e. V, Michael Faraday Strasse 1, Hermsdorf, 07629 Germany*

**e-mail: Steve.Tennison@mastcarbon.co.uk*

Abstract—A novel route is described for the production of carbon-ceramic membranes where the structure can be adjusted for use in either multiphase (gas–liquid) or gas phase membrane reactors. The production route allows the deposition of the membrane layer onto a two layer ceramic support (1OO nm top layer) giving potentially significant cost savings. It has also been shown that the route can be readily extended to multichannel monolith supports allowing a simple scale up route. The carbon component also provides an excellent support for the active metal allowing the production of high metal dispersions.

DOI: 10.1134/S002315840706016X

INTRODUCTION

This paper examines the factors involved in the use of carbon-ceramic composite membrane systems in catalytic membrane reactors (CMRs) from the standpoints of the membrane requirements and membrane production and the preparation of a novel catalytic membrane system for use in multiphase hydrogen peroxide production. The potential of the system for use in gas phase CMRs will also be discussed.

There are a wide variety of different approaches to CMRs that have been covered in many reviews (e.g., [1]) and where the constraints are common to all membrane systems. Two specific types of membrane reactors can be identified that have very different structural requirements:

1. Gas phase reactors where the benefits primarily derive from the selective removal of a component to shift equilibrium (e.g., hydrogen) or the selective addition of, for instance, oxygen for safety reasons. These systems require a highly selective membrane layer with pores typically in the range 0.3–1 nm.

2. Multiphase reactors where the membrane is used to separate the gas and liquid phases. In this case the pore size is fixed by capillary forces that maintain the gas–liquid interface at a fixed point within the membrane. In this instance significantly larger pores, typically tens of nm, are beneficial.

These can then be further subdivided depending on where the catalyst is located, within the membrane system or as free standing catalysts inside or outside of the membrane tube. This paper will concentrate on carbon-ceramic composite membrane systems where the catalyst is located within the membrane and where the carbon component is critical in providing both the support for the metal catalyst and as a means of modifying the pore structure of the membrane system.

The level of research into ceramic membrane systems has continued to increase over the last few years reflecting the limitations imposed by polymer membranes, and this has extended to the potential use of the ceramic membranes in membrane reactor systems. There have been several recent reviews of carbon membranes (e.g., [2, 3]) that have examined the wide variety of physical forms and methods of production that are available. These have demonstrated the flexibility of carbon membrane systems but have also highlighted some of the problems that are, in many cases, common to all ceramic membranes.

The main factors controlling the use of membrane systems can be identified as follows:

(1) Performance—defined by flux and selectivity. In polymer membranes, where the performance is generally controlled by a solution/diffusion mechanism, the flux and selectivity are interrelated and reflected in the well-known Robeson plots [4]. In contrast, ceramic membrane performance is controlled by a combination of micropore multicomponent adsorption and multicomponent diffusion where the nature of the performance strongly depends on a combination of pore size, concentration, pressure, and temperature.

(2) Stability—resistance of the membrane to the chemical and physical (pressure/temperature) environment. Polymeric membranes are limited in their operating temperature to perhaps 150°C, and high pressures can accelerate collapse due to plasticization by the feed components. In contrast, the ceramic membrane can be used to high temperatures, limited only by the stability

[1] This article was submitted by the authors in English.

of the micropore structure, and very high pressures. These properties are crucial to their use in membrane reactors.

(3) Cost—this relates to a combination of intrinsic cost of the membrane material and the module and installation costs which are a function of the ratio of the membrane surface area: module volume and the operating conditions. Modern hollow fiber polymer membrane modules achieve >10000 m^2/m^3 in marked contrast to a maximum of ~200 m^2/m^3 achievable with monolithic ceramic systems. Module costs for polymer systems are typically \$20–25 m^2 whilst this is around \$1500–2000 m^2 for ceramic liquid phase filtration modules and estimated at >\$3000 m^2 for zeolite-based gas separation membranes [5].

(4) Manufacturability—over 10^6 m^2/year of polymer membranes are now produced with a high degree of reliability and reproducibility reflecting the continuous low temperature production process [6]. Studies have shown that the presence of pores of ~0.5 nm width covering only one-millionth of the surface would render the membrane ineffective [7, 8]. In contrast, current nanoporous gas separation membranes typically comprise a 4 to 6 layer ceramic structure that requires a high temperature (>1200°C) firing stage after each layer deposition and, for zeolite membranes, an autoclave synthesis stage that can take in excess of 72 h. Reproducibility is often poor, and even under carefully controlled laboratory conditions, it is difficult to achieve a yield of >70% of acceptable membranes [9].

Polymeric membrane gas separation systems have made a major impact in several gas separation applications and now account for a significant part of the natural gas separation and nitrogen production processes [10], where the properties, as defined above, give rise to cost effective process solutions. Their further expansion is however constrained by their poor physical and chemical stability and limited selectivity–flux relationship. These also limit their use to a very small subset of possible membrane reactor applications. Ceramic membranes can overcome these limitations but at greatly increased cost. In polymer membranes the high flux is achieved by generating an asymmetric structure comprising a macroporous support that provides the mechanical stability combined with a very thin nonporous selective surface layer usually through a solution casting—coagulation mechanism [11, 12]. The overall diameter of the spun hollow fibers is typically of the order of 200 μm, while the thickness of the separating layer is around 1–200 nm. The goal in carbon and ceramic membranes has been to replicate this structure.

The challenge in the gas separation ceramic membranes is twofold:

(1) The requirement to form a "defect free" separating layer with a thickness approaching that achieved in the polymer membranes.

(2) The requirement for a support system that can provide the necessary combination of gas transport and mechanical strength and to achieve these at an acceptable cost.

The strength requirements have led most groups to use tubular or monolithic supports where the wall thickness is typically 1–2 mm. This thickness imposes severe gas transport limitations that have, in turn, led to the use of multilayer ceramic systems where the majority of the substrate is formed from large particle size α-alumina leading to high porosity (~35%) and pores in the 1–4 μm range. A series of smaller particle size layers is then formed on the surface to eventually create a nanoporous filtration membrane usually produced from, for instance, γ-alumina, titania, or zirconia. This structure can then be used as a support for the gas separation layer which is usually formed from either zolites that are grown in situ or amorphous silica. The structure of a multilayer tube produced by HITK (Hermsdorfer Institut für Technische Keramik) is shown in Fig. 1. In this membrane the tube is 10 mm in diameter with a wall thickness of 1.5 mm comprising sintered α-alumina particles with pores of 3 μm and 30% porosity [13]. The second α-alumina slip cast layer can have pores between 60 and 200 nm and detailed studies have shown that defect-free structures at this stage, as reflected in the bubble point, can only be achieved through a two stage process giving a layer thickness of ~50 μm. For gas separation membranes, a further nanoporous layer is then required. Colloidal sol gel processes can reduce the pore size to ~2 nm while a polymeric sol gel process can potentially reduce this to less than 1 nm for both titania [14] and silica surface layers. The alternative is to develop a gas separation zeolite layer on [9] or in [15] the 2 nm nanoporous top layer. The multiple coat–fire cycle at >1250°C is responsible for the high cost of these materials and also for potential problems with defects.

An alternative solution, which has been quite widely explored, is the use of sintered stainless steel supports [16]. These have the benefit that construction of high temperature modules can be achieved through usual engineering methods. The main drawback is that it is not possible to form the multilayer supports that are required to provide the combination of high permeability along with the nanopore structure that is essential for supporting the gas separation membrane.

A further approach that has attracted more attention recently is the production of hollow fiber structures produced by a phase inversion process analogous to those used in the polymer systems [17]. The process typically uses fine grain alumina dispersed into a polymer solution such as polyether sulfone that is spun into fibers that are then fired at high temperature (~1500°C) to generate the ceramic fiber. The surface structure comprises 0.3 μm particles and pores, which is similar to the structure achieved after the first layer deposition in the conventional process. These can then be used as substrates for the generation of the microporous gas separation layers, although this required up to 4 coats

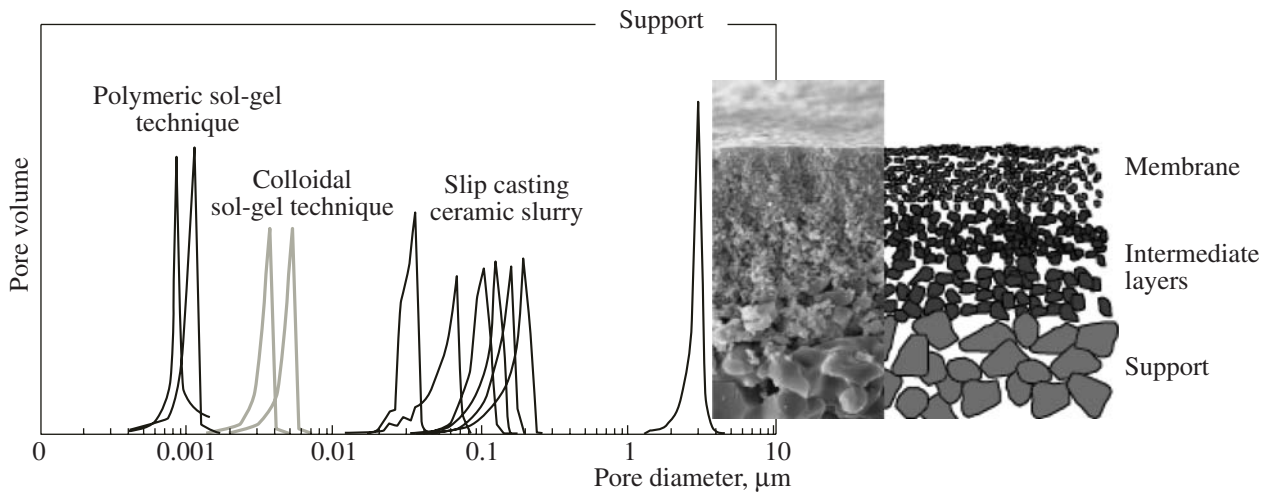

Fig. 1. Structure of HITK multilayer ceramic support system.

and a total deposition time of in excess of ~250 h to potentially achieve defect-free gas separation membranes. A further problem with the fiber systems is the construction of the module. While in polymer membrane systems this is not a problem, as polymeric potting compounds can be used in ceramics membranes, where the operating conditions are expected to be far more severe, a satisfactory solution has yet to be found.

Carbon membrane systems have the same sets of constraints as the ceramic systems with the requirement for a mechanically stable support, and this has lead to the investigation of a similar set of systems to those used for the oxide membranes—on [18] or in [19] porous ceramics, with sintered stainless [20], and in addition with macroporous graphite [21]. There has also been a significant interest in hollow carbon fibers where the membrane is formed directly from the asymmetric hollow polymer fiber membranes. While at first sight this would seem to be an ideal way of generating the required asymmetric structure directly, it has so far proved difficult to generate defect-free membranes in a single step without the addition of a secondary polymer layer to block the defects [22], although very careful control of the pyrolysis process has lead to improvements [23]. The problems of mounting these thin and fragile fibers in modules continues to be a significant problem.

The structure requirements for multiphase membranes are different in that the high selectivity gas separation layer is no longer required and can actually be detrimental to the overall performance. The performance of these systems requires that the gas–liquid interface is close to the liquid feed side of the membrane to minimize mass transfer limitations in the liquid phase while any possibility of gas escape from the gas phase to the liquid phase must be minimized. This is achieved by utilizing capillary forces. When first immersed in the liquid phase, the membrane system will fill with liquid. If pressure is then applied to the large pore size of the membrane, the liquid will be forced from the larger pores at the pressure determined by the Laplace equation.

In an idealized multilayer structure, this would result in the gas–liquid interface then sitting at the interface between the two pore systems. At a higher pressure, the interface can then be moved to the next pore structure interface. This mode of operation imposes an absolute requirement for a minimum of a two layer structure where the size of the smaller pores is fixed by the pressure drop that is required across the system. This also imposes an absolute limit on the size of any defects that can be tolerated in the outer layer.

As discussed, the critical factor in the production of viable (cost vs. performance) ceramic membranes derives from the combination of the support cost, the ease of manufacture, and the performance. It has been shown in several studies that high quality ceramic gas separation membranes can only be produced on or in a substrate with pores of a maximum of 5 nm with no defects larger than this size, which can only be achieved through an expensive multilayer structure.

In contrast, a major benefit of the carbon-ceramic composite membranes is the ability to produce a highly selective membrane directly on a macroporous support. In one of the first published examples, Rao et al produced highly selective carbon membranes by coating a polyvinylidene chloride latex onto an alumina disc with pores in the range 0.3–1 μm to give a 2–5 μm carbon film. In the first studies this required multiple polymer coat–carbonization studies to give good separation performance [24]. The multiple coat-carbonize cycles insured that the subsequent coats blocked the defects in the previous layer introduced during the pyrolysis cycle. The defects were due to the shrinkage that occurs during polymer pyrolysis, which frequently exceeds 50% volume [25]. However, the defect problem appears

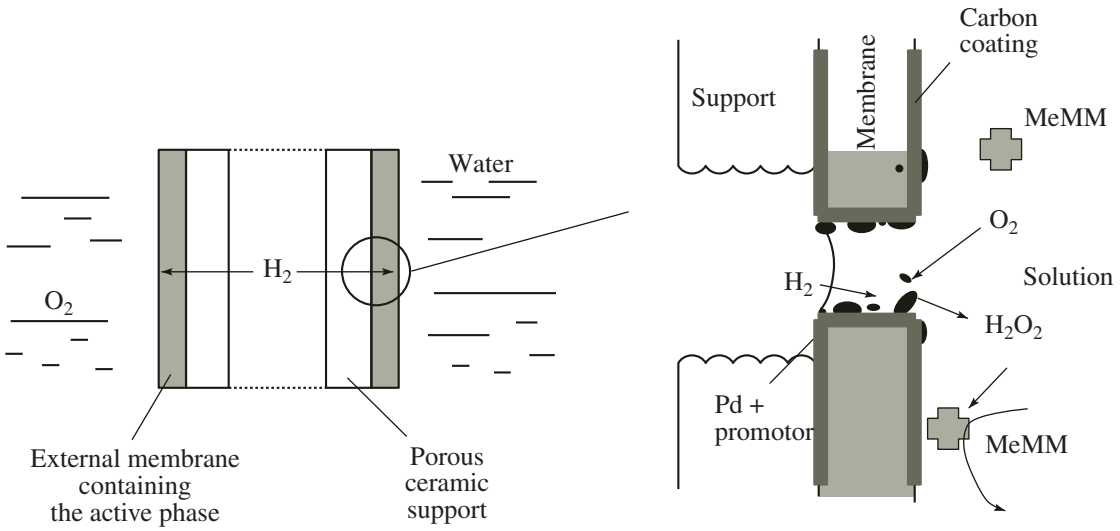

Fig. 2. Multiphase membrane structure and mode of operation.

to be restricted to thicker films and it seems from several studies that where the film is very thin, ~5 μm, it can accommodate this shrinkage without the production of defects. This is reflected in the later results of Rao et al where the production was improved to a single coat–carbonization cycle on homogeneous alumina tubes with pores of ~1 μm [26]. The resulting carbon membranes had pores of around 0.5 nm and gave very good gas separation by what Rao et al termed "selective surface flow." The clear benefit of this system was the ability to use a homogeneous macroporous alumina support and a single polymer coat-carbonize cycle with clear implications for the cost of the membranes. Since these early studies, a significant amount of work has been carried out that has been fully reviewed by Ismail et al. [2, 3]. Fuertes et al have investigated the use of Novolak phenolic resin as the carbon precursor on ceramic substrates. In their initial studies they used macroporous graphite supports with a pore size of around 1 μm to support 1–2 μm thickness PVDC [27] and phenolic resin [28] derived membranes that showed excellent molecular sieve separation characteristics. However, their subsequent studies moved to the more conventional four-layer ceramics where the outer layer comprised γ-alumina with 5 nm pores. Other than the benefits of the tubular structure and a simple dip and drain preparation route, the shift to this more complex support gave almost no benefits in terms of permeability (8×10^{-9} mol m^{-2} (s Pa)$^{-1}$) and virtually identical selectivity for CO_2/CH_4 of around 150–160. Carretero et al. [19] also used Novolak phenolic resin and a multilayer ceramic support although in this instance the resin was impregnated γ-Al_2O_3 into the γ-alumina top layer where the substrate comprised a 2.7 μm pore cordierite base layer, a 90 nm pore size intermediate γ-alumina layer, and 3 layers of ~4.5 nm pore γ-alumina. The resin film was infiltrated into the 7-alumina top layers which was then carbonized at 700°C. In this case the fully infiltrated carbon membrane was ~4 μm thick and had a permeance of ~3×10^{-9} mol/(m^2 s Pa).

Several workers have also demonstrated the way in which the properties of the carbon membrane layer can subsequently be modified by adjusting the carbonization conditions [29], through preoxidation of the polymer and by careful post oxidation of the carbon layer [30]. In general, however, post oxidation, while increasing the permeability of the membrane, leads to a significant decrease in selectivity.

Future developments in the ceramic membrane field must be to achieve the control of both the support and membrane structure required by the target application while also minimizing the cost of the overall system through a production route compatible with large scale manufacture. This almost certainly implies the ability to move from the simple tubes used in the most current studies to the multichannel monoliths that will be essential to achieve acceptable surface : volume characteristics.

The work reported here is also based on a phenolic resin precursor but is based on a relatively simple two-layer ceramic support structure to minimize costs. This has allowed the properties of the carbon-ceramic system to be modified over a wide range of porosities compatible with both the gas phase and 3-phase membrane reactor applications. The presence of the high surface area glassy carbon layer has also allowed the controlled production of both mono- and bimetallic catalytic membrane systems that have shown good performance for the in situ generation of hydrogen peroxide. The catalytic performance of these membrane systems has been reported elsewhere [31–33], and this paper will concentrate on the production and properties of the membranes. The production route has also been extended to multichannel monoliths.

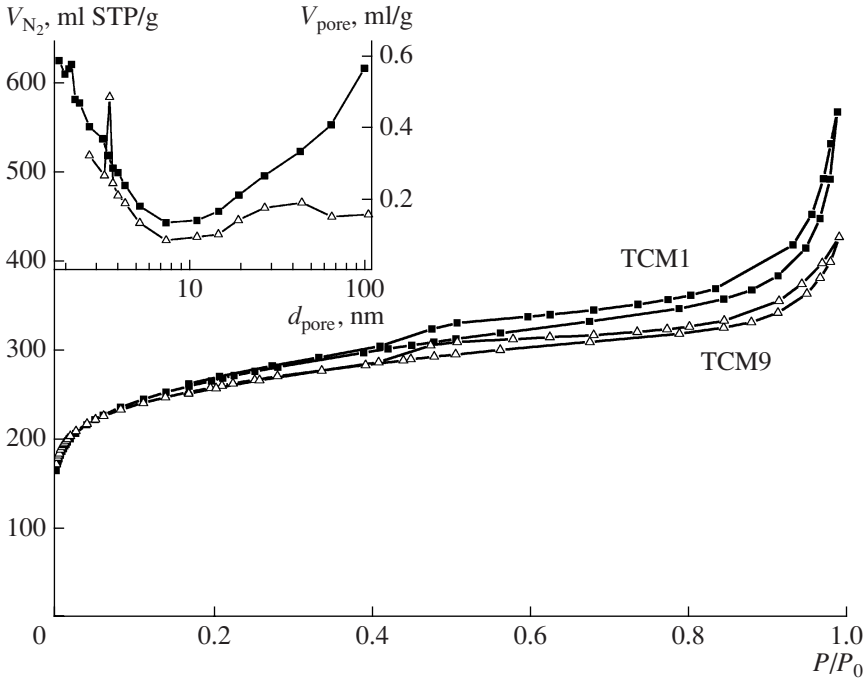

Fig. 3. Pore structure of the carbon ceramic composite membrane top layer by nitrogen adsorption (from reference (33)).

EXPERIMENTAL

Membrane Production

The primary goal of work [34] was to generate a catalytic membrane reactor system for use in the reaction

$$H_2 + O_2 \longrightarrow H_2O_2.$$

The role of the membrane system is to separate the hydrogen and oxygen as shown in Fig. 2 where the oxygen is dissolved in the liquid phase. In this system there is no need for a highly selective membrane layer. The separation of the gas and liquid phases is achieved entirely through the graded pore structure through capillary forces. This can be seen from the Laplace expression for the bubble point [35]:

$$BP = \frac{2\delta\cos\theta}{d/2},$$

BP is bubble point in bar; δ is surface tension, N/m^2; θ is contact angle; d is diameter of pore or defect, m.

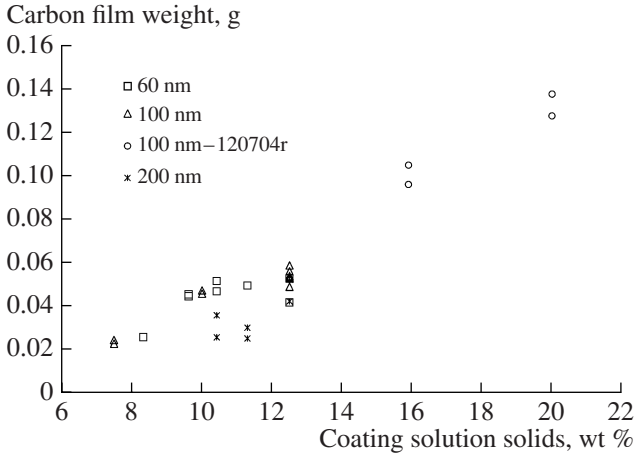

Fig. 4. Carbon loading on the two-layer HITK ceramic support as a function of the nanoporous layer pore size (1st Series Resin).

As the pressure on the large pore side of the membrane is increased at a certain pressure, this part of the pore structure will be completely emptied and the gas–liquid interface will be at the interface between the macroporous and the nanoporous layers. For water and a zero contact angle, this would occur at ~1.5 bar. At a much higher pressure, the liquid will eventually be displaced entirely from the nanoporous layer, for a 100 nm top layer this would occur at ~29 bar. Provided there are no defects, operation at pressures intermediate between these two levels will provide a stable operating regime. This also provides an ideal mass transport environment as only the hydrogen needs to diffuse through the thick support layer, while liquid diffusion is limited to the much thinner nanoporous layer. Due to the diffusion limitations in the liquid phase, the reaction only takes place close to the gas–liquid interface and it is therefore important that the catalyst is primarily located in this regime. Both the support and the nanoporous layer comprise low surface area α-alumina which is not ideal as a catalyst support and can also catalyze the decomposition of the peroxide. There was, therefore, a requirement to coat all parts of the alumina structure

Table 1. Characteristics of ceramic membrane support tubes

	Ceramic permeance		Ethanol bubble point	
	$m^3/m^2/s/mbar$	variation	bar	variation
Single outside coat, 1250°C (5)	$(7.9 \pm 1.4) \times 10^{-5}$	17.7	0.92 ± 0.26	28
Double outside coat, 1250°C (5)	$(6.33 \pm 1.1) \times 10^{-5}$	17.2	3.02 ± 1.33	44
Single outside coat, 1200°C (20)	$(8.70 \pm 2.0) \times 10^{-5}$	22.8	1.5 ± 1.0	65
Single outside coat, 1250°C (5)	$(9.80 \pm 2.4) \times 10^{-5}$	24.3	2.1 ± 0.7	32
Single outside, 1250°C, glazed (4)	$(6.9 \pm 0.5) \times 10^{-5}$	7.8	0.92 ± 0.26	–
Double inside coated, 1250°C, glazed (5)	$(4.25 \pm 0.35) \times 10^{-5}$	8.3	>5	–
Double inside coated, 1250°C, glazed (6)	$(5.6 \pm 0.27) \times 10^{-5}$	5.0	–	–
Double outside, 1250°C, (4) selected	$(5.8 \pm 0.3) \times 10^{-5}$	5.0	–	–
Double outside, 1250°C, (3) selected	$(6.1 \pm 0.5) \times 10^{-5}$	8.4	–	–

* No in brackets shows number of membranes in the sample.

with carbon without significantly reducing the permeability of the structure.

The route chosen was to use phenolic resin but, in contrast to most other workers who have used Novolaks, this was based on a Resol resin. While both resins will ultimately give a similar carbon structure, Novolaks are thermoplastic polymers that require a secondary curing agent, usually hexamethylene tetramine (HEX), to produce the cross linked resin. This has the disadvantage that temperatures above ~120°C are required to initiate the cure and there is significant gas evolution associated with the HEX decomposition. In contrast, Resols are intrinsically active and only require gentle heating to complete the cure reaction allowing more precise control of the cure cycles.

The support tubes were supplied by HITK and comprised a 10 cm long, 1 cm OD, 1.7 mm wall α-Al_2O_3-alumina tube with either a single or double fine grain external α-alumina surface layer with either 200, 100, or 60 nm pores. Some tests were also carried out with internally coated tubes and multichannel monoliths with 100 nm top layers. The resol resin (J2225S supplied by Hexion) was supplied as a 50% weight solid in ethanol solution. This was then further diluted with either acetone, methanol, ethanol, or isopropanol to give the required coating concentration. The tubes were immersed in the coating solution in a container inside a dessicator. This was carefully evacuated and repressurized twice to insure that the solution fully penetrated the ceramic structure. The excess solution was then drained from the tube which was then dried in an air oven overnight at 40°C, followed by a ramp cure cycle in a temperature controlled oven to 120°C over 6 h. The critical requirement in this cycle is to ensure that the solvent is removed before the resin is significantly cross linked. Solvent release from a partially cured resin can lead to bubble formation and inferior coatings. The different solvents were examined to assess whether this had an impact on the rate of solvent removal. The best results were obtained with isopropanol, which was used for the majority of the experimental preparations. In some cases a second resin coating was applied in the same manner after the curing cycle. The cured membranes were then carbonized and activated. In some cases this was in nitrogen at 800°C, followed by carbon dioxide at 850°C for varying times, or alternatively this was carried out in a single step direct to the required activation conditions, usually CO_2 at 850°C for 1 h.

The nitrogen permeance of the coated tubes was determined after carbonization and also occasionally after the resin coating stage. Hydrogen and SF_6 permeances were determined by HITK along with scanning electron microscopy of the carbon-coated tubes.

Catalyst deposition and testing were carried out by the University of Venice, and the methods of preparation and the membrane test procedure have been reported elsewhere [31–33]. The catalysts included both Pd and Pd/Pt bimetallic systems.

RESULTS AND DISCUSSION

The initial tests established the preferred coating conditions (one or two layers and the coating solution concentration). Using 12.5% weight resin solids in IPA solution gave very good reproducibility with resin deposition on the 10 cm tubes of 1.01 ± 0.06% weight giving rise to carbon loading of 0.050 ± 0.003 g/tube and a carbon yield of 45.3 ± 3.2% over an 11 tube series following treatment in carbon dioxide at 850°C for 1 h which resulted in ~20% weight loss by activation from the carbonized structure. Even so, a slight trend was observed in mass along the series that was attributed to the sequential production of the tubes and a resulting decrease in the solution resin concentration. The pore

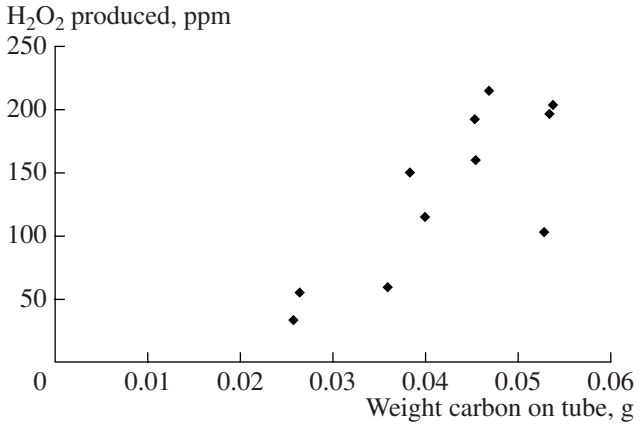

Fig. 5. Hydrogen peroxide production as a function of carbon weight loading for the palladium-catalyzed membrane system.

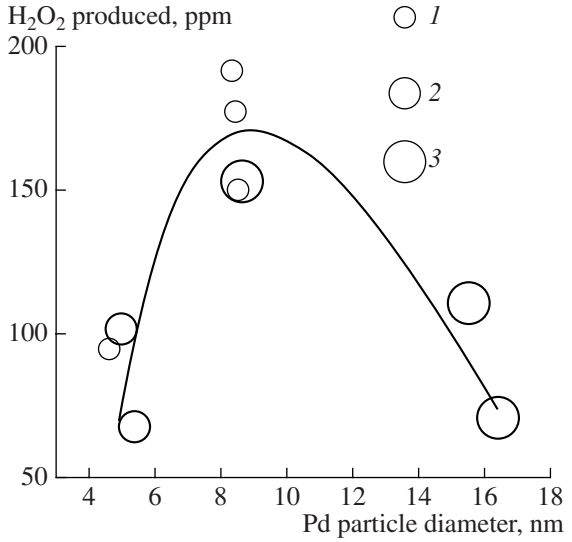

Fig. 6. Structure sensitivity of palladium-catalyzed hydrogen peroxide formation (from reference (33)). The amount of Pd is (*1*) 0.9–1.1, (*2*) 1.1–1.5, and (*3*) >1.5 mg.

structure of the membrane surface was analyzed by nitrogen adsorption using a Micromeritics ASAP 2000 and small chips from the membrane top layer. This clearly shows (Fig. 3) the macropore structure that derives from the carbon-coated 100-nm substrate and the micro/meso pore structure within the actual carbon film. The surface area of the resulting carbons, after processing at 850°C for 1 h, was in the range 584 to 845 m^2/g. The mesopore structure is particularly significant for catalyst support use as carbons derived from phenolic resins are generally extremely microporous.

Thereafter all tubes in a given set were impregnated simultaneously (up to 15 at one time) which reduced the error in the resin masses to less than ±3% compared to ±6%. The variation in the resin loading on the tubes as a function of solution concentration is shown in Fig. 4 for the three membrane top layer structures—60, 100, and 200 nm. This shows a linear increase in carbon loading with resin solids with little difference between the 60 and 100 nm pore systems but a small decrease in loading for the 200 nm system.

Despite the excellent reproducibility of the carbon loading process, the repeatability of the nitrogen permeance was much worse—$(1.0 \pm 0.45) \times 10^{-5}$ $m^3\ m^{-2}\ s^{-1}\ mbar^{-1}$ (45%). A detailed investigation of the support tubes suggested that this was due to defects present in the nanoporous layer. The bubble point and permeance characteristics of the range of support tubes where the firing temperature and number and location of the nanoporous layer were varied are shown in Table 1. It can be seen that the standard production route in use at the

Table 2. Effect of support pore structure on membrane performance

Pore Size	Resin Conc	HITK			MAST		
		H_2	SF_6	permselectivity (H_2/SF_6)	l/h/m^2/bar	H_2/N_2	$m^3/m^2/s/mbar$
60	12.5	27193	5590	4.86	18839	1.44	5.23×10^{-6}
60	10.4	1067.3	154	7.06	596	1.82	1.66×10^{-7}
60	9.6	2812	416	6.76	2790	1.01	7.75×10^{-7}
60	6.3	43457	9609	4.52	28375	1.53	7.88×10^{-6}
100	8.8	–	–	–	108360		3.01×10^{-5}
100	10.4	22182	3725	5.95	11664	1.90	3.24×10^{-6}
100	9.6	4605	727	6.33	2189	2.10	6.08×10^{-7}
Support	–	409601	74710	5.48	–	–	–
200	12.5	33284	6358	5.23	20700	1.61	5.75×10^{-6}
200	11.3	–	–	–	142200	–	3.95×10^{-5}
200	10.4	–	–	–	84240	–	2.34×10^{-5}

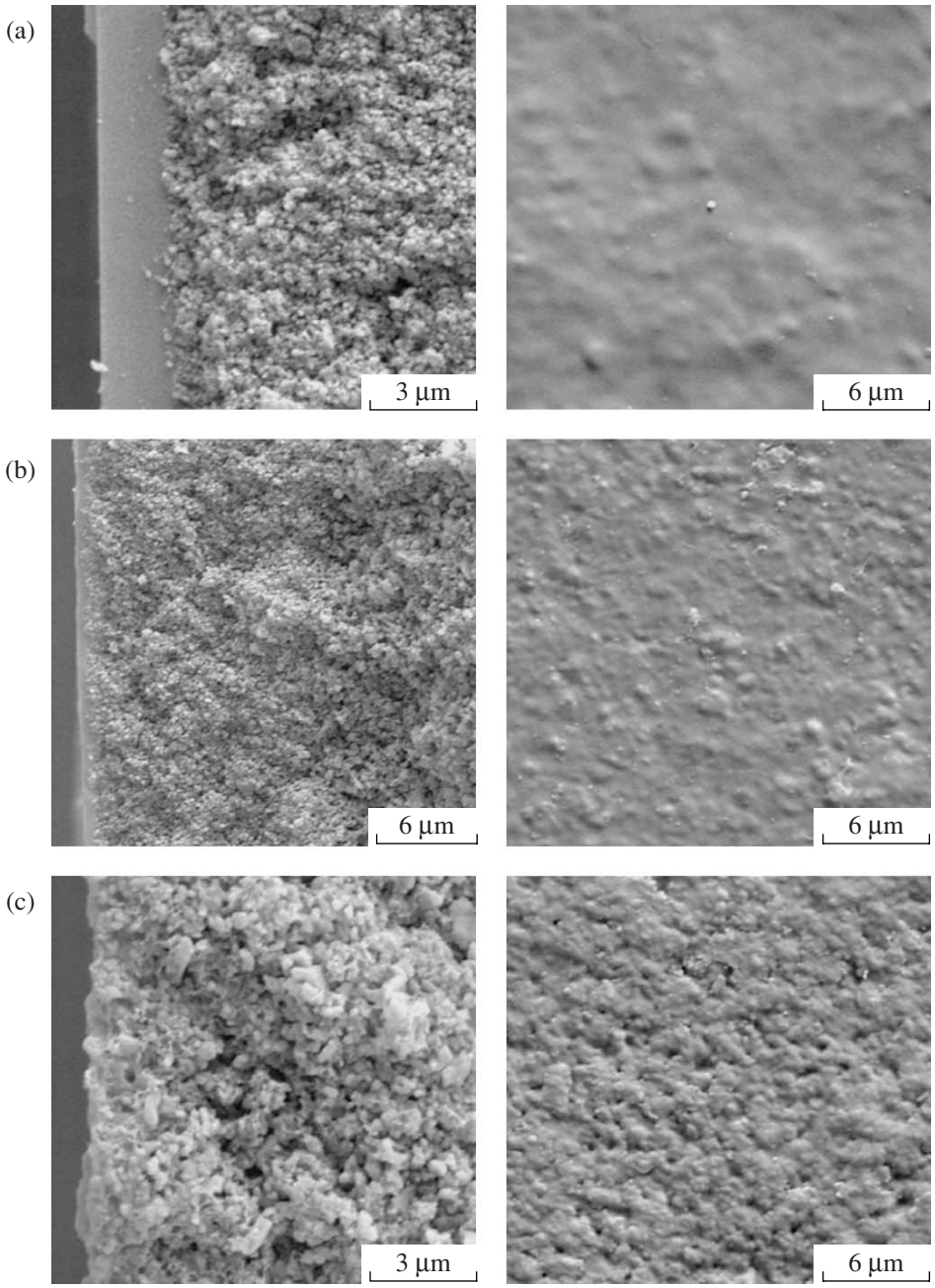

Fig. 7. SEM images of carbon surface structure of 1st series membranes showing variation in the surface carbon layer. (a) Low permeability 1087 l/(m^2 h bar); (b) medium permeability 4605 l/(m^2 h bar); (c) high permeability 33284 l/(m^2 h bar).

start of the program (external single layer, fired at 1200°C) or a firing temperature of 1250°C all gave quite poor permeance reproducibility but, more significantly, have very poor ethanol bubble points with a mean of around 1 bar and a very wide deviation. This can be compared with the expected bubble point for a 100-nm pore layer of >5 bar and demonstrates the presence of very significant defects. Moving to a double outside coat increased the mean to 3.0 bar but made little difference to the variance while, quite surprisingly, moving to a double internally coated tube gave rise to a major improvement with all tubes showing a bubble point >5 bar, although this was found too late to implement the change for the majority of the studies. After this the tubes used in the program were selected by bubble point and this resulted in the improved repeatability of ~5–8% shown in the Table 1. The variability of the early tubes has, however, had an impact on the initial tube performance characteristics.

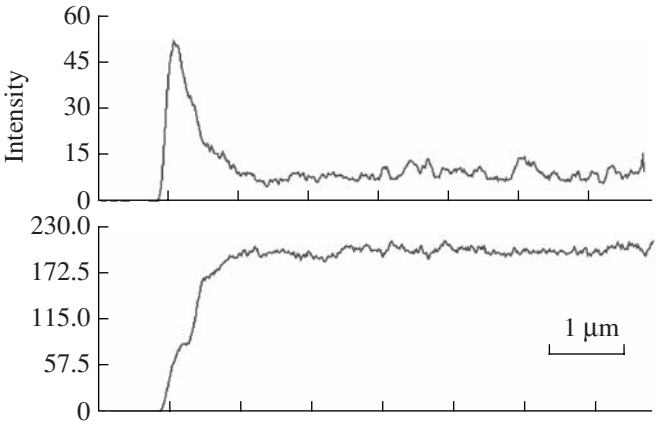

Fig. 8. EDAX analysis of carbon membrane showing the surface layer and distribution through the 100-nm substrate layer.

The tubes used in the study of the impact of layer pore size on loading were used to evaluate the peroxide production under standard conditions. The results are shown in Fig. 5 and show a steady increase in ppm H_2O_2 as the carbon loading on the membrane is increased. While it might be expected that this reflected an increase in palladium loading with carbon loading, no direct correlation was found in the later stages of the study. However, this may well be due to the complexity of the reactivity–palladium loading response which shows a strong structure sensitivity with optimum performance at intermediate particle sizes [32, 33] (Fig. 6). Clearly the ability of the carbon structure to allow optimum dispersion is critical to the overall performance of the membrane system.

The permeance of the membranes for hydrogen and SF_6, along with SEM and EDAX, were determined by HITK. These are compared with the MAST nitrogen data in Table 2 and with the SEM pictures in Fig. 7. Visually, the outer layer varied between a matte and a high gloss finish, the high gloss finish being due to the 2 μm carbon film that formed on the surface (Fig. 7); a thinner film is apparent in the intermediate flux membrane while the highest flux membrane shows essentially no surface film. This is also reflected in the surface roughness, which has largely been eliminated in the thicker membrane. Examination of the permeance data shows that the permselectivities are close to those of the uncoated 100 nm substrate for all except the membranes with significant surface layers, although it is surprising that this only rises to 7.05 for the 2-μm film membrane. EDAX analysis of the thick film membrane in Fig. 8 shows that within the alumina support the carbon is distributed evenly throughout the 100-nm alumina layer of the membrane.

As Fig. 5 showed a strong correlation with carbon weight loading, the subsequent samples, investigating the impact of carbon layer activation, were produced at a higher resin loading with a first stage carbonization in nitrogen at 800°C followed by treatments in carbon dioxide at 850°C for up to 2 h. The solution concentration of 20% weight was expected to give a carbon loading of 0.13 g (Fig. 5), but after a secondary treatment at 850°C for 1 h to match the preparative conditions for the first series, it gave only 0.11 g. The activation of the carbon is linear with time (Fig. 9), but this gives rise to an exponential increase in permeance (Fig. 10). The peroxide yield from these activated tubes (Fig. 11) is linear with the activation extent but falls into two distinct clusters. Although the two sets were made under nominally identical conditions, they can be differentiated by the weight of carbon on the tubes after the nitrogen carbonization stage even though the resin loading was identical. At present there is no explanation for this observation.

The visual appearance of these samples was also different from the earlier set in that all of the samples had a matte surface finish, despite the high carbon loading, and SEM showed no evidence for any surface film formation. This was also reflected in the film permeance which showed little change with carbon load-

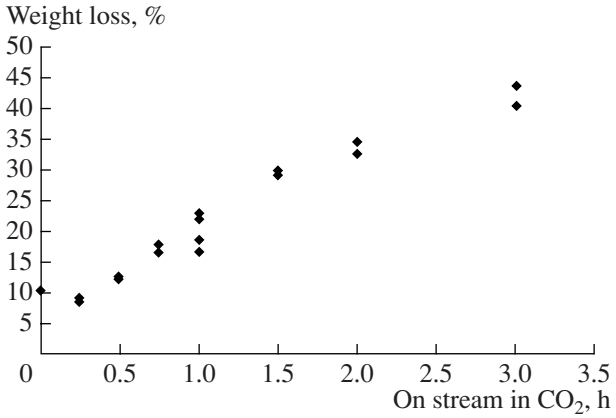

Fig. 9. Carbon dioxide activation of carbon layer on carbon-ceramic composite membrane.

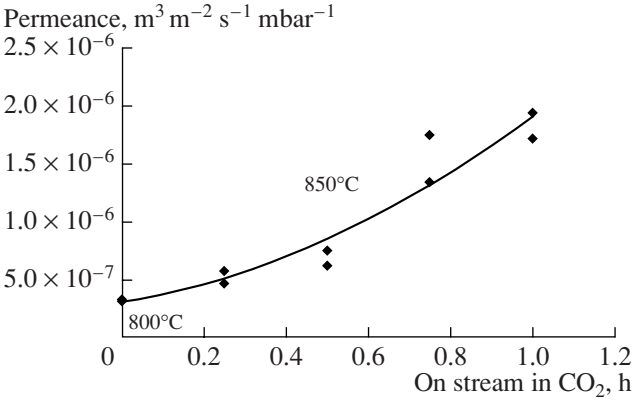

Fig. 10. Variation in permeance of the carbon-ceramic composite membrane with activation level.

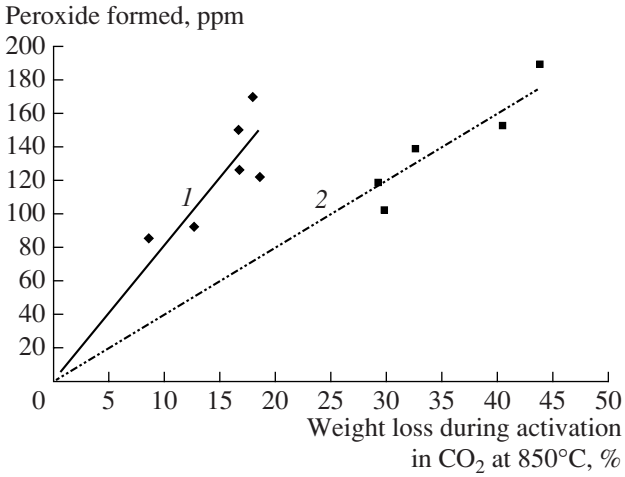

Fig. 11. Hydrogen peroxide production as a function of extent of activation (2nd series resin). The carbon content after carbonization in nitrogen at 850°C is (*1*) 1.32 and (*2*) 1.10 wt %.

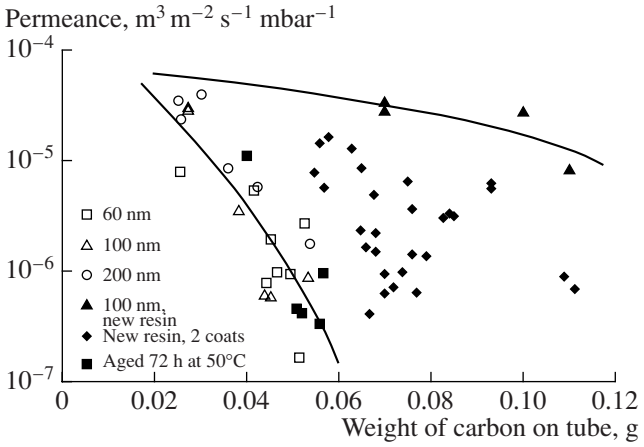

Fig. 12. Permeance of 2nd membrane series as a function of carbon weight loading and preparative conditions.

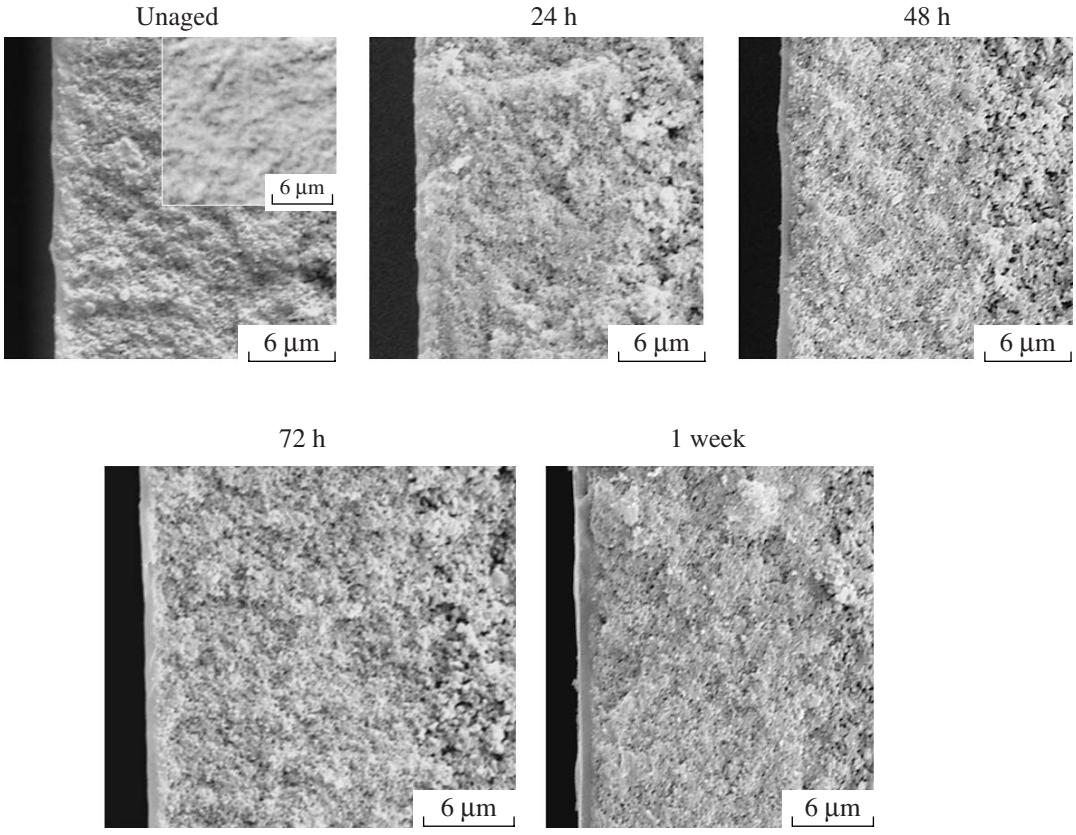

Fig. 13. SEM images of 2nd series membranes showing development of carbon surface layer as a function of resin ageing.

ing in marked contrast to the rapid reduction with loading exhibited in the first series (Fig. 12). It was also apparent that the peroxide yield was lower than seen in the first series of samples for a given carbon weight. The main change between these two series was that a new batch of resol resin was used. It appeared that the new resin had a much lower film-forming capability compared to the original resin, and GPC analysis showed that the older resin had probably partially polymerized despite being stored in a fridge. Two

Table 3. Performance characteristics of membranes based on new and aged resin

Support system	Coating no. × solution concentration	Resin ageing time (h) × temp	Process gas	Carbon loading, g	Permeance hydrogen			Permselectivity	
					H_2	N_2	SF_6	H_2/SF_6	H_2/N_2
1 coat 1200°C	2/10	–	N_2	0.113	2.53	–	0.01	303.3	–
1 coat 1200°C	1/12.5	–	N_2	0.072	4.09	–	0.04	98.2	–
1 coat 1200°C	1/20	–	N_2	0.138	2.53	–	0.03	82.8	–
1 coat 1200°C	1/15.9	–	N_2	0.096	9.25	–	0.70	13.3	–
2 inside, 1200°C	2/10	–	CO_2	0.093	775.39	–	113.58	6.8	–
2 inside, 1200°C	2/10	–	CO_2	0.093	807.56	–	97.81	8.3	–
1 coat 1200°C	2/10	24/40	CO_2	0.092	12.36	–	1.92	6.4	–
1 coat 1200°C	2/10	72/40	CO_2	0.097	14.67	–	2.39	6.1	–
1 coat 1200°C	2/10	168/40	CO_2	0.097	64.06	–	11.00	5.8	–
2 inside	2/10	72/40	CO_2	0.093	126.08	42.75	33.36	3.8	2.9
2 coats 1250°C	2/10	268/40	CO_2	0.118	38.81	11.31	6.14	6.3	3.4
1 coat 1200°C	2/7.6	72/50	N_2	0.104	6.14	1.11	0.61	10.0	5.5
1 coat 1200°C	2/7.6	72/50	N_2	0.103	5.03	0.03	0.01	603.3	150.8
1 coat 1200°C	2/7.6	48/50	N_2	0.098	4.47	0.04	0.01	536.7	123.8
1 coat 1200°C	2/11.2	48/50	N_2	0.094	2.81	0.03	0.02	168.5	84.3
1 coat 1200°C	2/10	24/50	CO_2	0.113	81.33	24.56	13.17	6.2	3.3
1 coat 1200°C	2/7.6	48/50	CO_2	0.080	189.27	56.75	29.33	6.5	3.3
1 coat 1200°C	2/11.2	72/50	CO_2	0.096	82.93	25.64	15.03	5.5	3.2

approaches were used to try and recover the original structure: the resin was artificially aged by holding the solution at up to 50°C for times up to a week and a two-coat procedure was adopted. Figure 12 shows the much higher permeance of the tubes made with the single coat new resin. The large scatter of points for the 2-coat procedure with the new resin largely reflects the use of a range of different concentrations in the first and second coat solutions, and while some of these approach the performance of the original resin, the permeance at specific carbon levels is still significantly higher. The final data set shows tubes prepared with the new resin solution that has been aged by holding it at 50°C for 72 h and a two-coat procedure. It can be seen that some of these now show equivalent performance to the old resin. Lower temperatures gave no benefit, while shorter times produced intermediate effects. The benefits of the ageing procedure can be seen clearly in the micrographs in Fig. 13, which shows the evolution of the film with time at 50°C. The evolution of the surface texture can also be seen in the inserts (Fig. 13).

The overall performance characteristics of these membranes are shown in Table 3. Several points emerge from this data. It can be seen that all of the tubes carbonized in nitrogen show dramatically reduced permeances and in most cases now show high permselectivities for both H_2/SF_6 and for H_2/N_2. Of the nitrogen processed tubes, it can also be seen that the membranes made with the aged resin show the highest permeances and selectivities. The best hydrogen permeance 5×10^{-10} m^3 m^{-2} s^{-1} Pa^{-1} compares favorably with other values reported in the literature, while the H_2/N_2 permselectivity (150) is significantly higher. It seems likely that higher performance should be attainable by more precise control of the carbonization conditions, which have yet to be optimized. The table also shows the very marked impact of activation on the permeance and selectivity. Processing under carbon dioxide for 1 h at 850°C leads to ~20% weight loss compared to the nitrogen processed tubes. This leads to a dramatic increase in permeance that is least marked for the tubes based on aged resin, although in all cases, as seen in the tubes

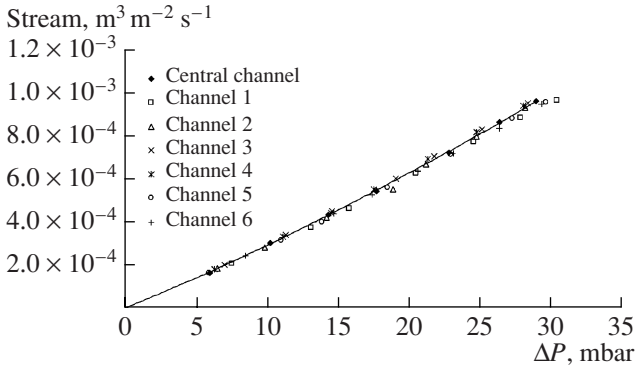

Fig. 14. Multichannel monolith membrane system: reproducibility of coatings within the channels.

made from the original resin, the permselectivity has returned to a value close to that expected for Knudsen diffusion. Catalytic tests in Venice using the tubes prepared from resin aged at higher temperatures showed that the productivity of the catalyst increased with ageing severity. This appeared to be due to very low peroxide decomposition activity rather than to an increase in the peroxide synthesis rate.

While the inside-coated, CO_2 processed tubes have a much higher permeance than equivalent outside-coated tubes for a given carbon content, SEM still showed the formation of a clearly defined surface carbon layer. On this basis the dip and drain technique was used to internally coat a 25 cm × 7 channel (100 nm surface layer) monolith using the 2-coat procedure. The permeance of each channel was then measured individually. The results (Fig. 14) show excellent reproducibility between the channels and demonstrate that this methodology can readily be applied to the multichannel systems.

CONCLUSIONS

These studies have shown that it is possible to produce a membrane system that is potentially suitable for use in both multiphase and gas phase membrane reactor systems based on a 2-layer ceramic substrate. In addition the production methodology can readily be expanded to multichannel monoliths allowing a facile route to scale up. The predicted costs for the system should be below \$1000 m^{-2}. The performance is, however, sensitive to the degree of perfection of the support, and good membrane results were only achieved by either the use of two ceramic coats to reduce defects or by preselecting the substrates based on bubble point. However, bubble point testing of the carbon-coated tubes showed a marked improvement in performance with most of the tubes tested then showing no defects (ethanol bubble point of >5 bar).

The carbon deposited within the nanoporous layer of the substrate has the structure and surface area to enable high dispersions of catalyst metals to be achieved when oxidized in carbon dioxide that have shown good performance in the direct synthesis of hydrogen peroxide.

When prepared under nitrogen, the carbon membrane later shows excellent gas separation characteristics despite the simple production route. Further improvements should be feasible by optimization of the carbonization conditions.

ACKNOWLEDGMENTS

Financial support from the EU (contract GR5D-CT2002-00678) is gratefully acknowledged. The authors are indebted to Dr. S. Melada and Professor G. Strukul (University of Venice) for the catalyst performance information.

REFERENCES

1. McLeary, E.E., Jansen, J.C., and Kapteijn, F., *Microporous Mesoporous Mater.*, 2006, vol. 90, nos. 1–3, p. 198.
2. Ismail, A.F. and David, L.I.B., *J. Membr. Sci.*, 2001, vol. 193, no. 1, p. 1.
3. Saufi, S.M. and Ismail, A.F., *Carbon*, 2004, vol. 42, no. 2, p. 241.
4. Singh, A. and Koros, W.J., *Ind. Eng. Chem. Res.*, 1996, vol. 35, p. 1231.
5. Caro, J., Noack, M., et al., *Microporous Mesoporous Mater.*, 2000, vol. 38, no. 1, p. 3.
6. Wallace, D.W., Staudt-Bickel, C., et al., *J. Membr. Sci.*, 2006, vol. 278, nos. 1–2, p. 92.
7. Henis, J.M.S. and Tripodi, M.K., *J. Membr. Sci.*, 1981, vol. 8, p. 233.
8. Koros, W.J. and Fleming, G.K., *J. Membr. Sci.*, 1993, vol. 83, p. 1.
9. Noack, M., Kolsch, P., et al., *Microporous Mesoporous Mater.*, 2001, vol. 49, nos. 1–3, p. 25.
10. Koros, W.J. and Mahajan, R., *J. Membr. Sci.*, 2000, vol. 175, no. 2, p. 181.
11. Wallace, D.W., Staudt-Bickel, C., and Koros, W.J., *J. Membr. Sci.*, 2006, vol. 278, nos. 1–2, p. 92.
12. Qin, J. and Chung, T.-S., *J. Membr. Sci.*, 1999, vol. 157, no. 1, p. 35.
13. Richter, H., Voigt, I., Fischer, F., Puhlfürß, P., and Köhler, B., *Int. Conf. on Catalytic Membrane Reactors*, 2006.
14. Puhlfürß, P., Voigt, A., Weber, R., and Morbé, M., *J. Membr. Sci.*, 2000, vol. 174, p. 123.
15. Miachon, S., Landrivon, E., Aouine, M., et al., *J. Membr. Sci.* (in press).
16. Au, L.T.Y., Chau, J.L.H., et al., *J. Membr. Sci.*, 2001, vol. 183, no. 2, p. 269.
17. Liu, S. and Li, K., 2003, *J. Membr. Sci.*, 2003, vol. 218, nos. 1–2, p. 269.
18. Centeno, T.A. Vilas, J.L., et al., *J. Membr. Sci.*, 2004, vol. 228, no. 1, p. 45.
19. Carretero, J., Benito, J.M., et al., *J. Membr. Sci.* (in press).

20. Shiflett, M.B. and Foley, H.C., *Carbon*, 2001, vol. 39, no. 9, p. 1421.
21. Fuertes, A.B. and Centeno, T.A., *J. Membr. Sci.*, 1998, vol. 144, nos. 1–2, p. 105.
22. Petersen, J. Matsuda, M., et al., *J. Membr. Sci.*, 1997, vol. 131, nos. 1–2, p. 85.
23. Itoh, N. and Haraya, K., *Catal. Today*, 2000, vol. 56, nos. 1–3, p. 103.
24. Rao, M.B. and Sircar, S., *J. Membr. Sci.*, 1993, vol. 85, no. 3, p. 253.
25. Tennison, S.R., *Appl. Catal., A*, 1998, vol. 173, no. 2, p. 289.
26. Anand, M. Langsam, M., et al., *J. Membr. Sci.*, 1997, vol. 123, no. 1, p. 17.
27. Centeno, T.A. and Fuertes, A.B., *Sep. Purif. Technol.*, 2001, vol. 25, nos. 1–3, p. 379.
28. Centeno, T.A. and Fuertes, A.B., *J. Membr. Sci.*, 1999, vol. 160, no. 2, p. 201.
29. Centeno, T.A. Vilas, J.L., et al., *J. Membr. Sci.*, 2004, vol. 228, no. 1, p. 45.
30. Fuertes, A.B. and Menendez, I., *Sep. Purif. Technol.*, 2002, vol. 28, no. 1, p. 29.
31. Abate, S. Centi, G., et al., *Catal. Today*, 2005, vol. 104, nos. 2–4, p. 323.
32. Melada, S. Pinna, F., et al., *J. Catal.*, 2006, vol. 237, no. 2, p. 213.
33. Melada, S. Pinna, F., et al., *J. Catal.*, 2005, vol. 235, no. 1, p. 241.
34. *EU Project "NEOPS,"* G5RD-CT-20020-00678.
35. Jakobs, E. and Koros, W.J., *J. Membr. Sci.*, 1997, vol. 124, no. 2, p. 149.